# $Ca^{2+}$ Signals in $CD4^+$ T Cells during Early Contacts with Antigen-Bearing Dendritic Cells in Lymph Node[1]

**Sindy H. Wei,* Olga Safrina,* Ying Yu,* Kym R. Garrod,* Michael D. Cahalan,[2]*† and Ian Parker*‡**

**T cell activation by APC requires cytosolic $Ca^{2+}$ ($[Ca^{2+}]_i$) elevation. Using two-photon microscopy, we visualized $Ca^{2+}$ signaling and motility of murine $CD4^+$ T cells within lymph node (LN) explants under control, inflammatory, and immunizing conditions. Without Ag under basal noninflammatory conditions, T cells showed infrequent $Ca^{2+}$ spikes associated with sustained slowing. Inflammation reduced velocities and $Ca^{2+}$ spiking in the absence of specific Ag. During early Ag encounter, most T cells engaged Ag-presenting dendritic cells in clusters, and showed increased $Ca^{2+}$ spike frequency and elevated basal $[Ca^{2+}]_i$. These $Ca^{2+}$ signals persisted for hours, irrespective of whether T cells were in contact with visualized dendritic cells. We propose that sustained increases in basal $[Ca^{2+}]_i$ and spiking frequency constitute a $Ca^{2+}$ signaling modality that, integrated over hours, distinguishes immunogenic from basal state in the native lymphoid environment.** ***The Journal of Immunology*****, 2007, 179: 1586–1594.**

To sustain adaptive immunity, a pool of naive $CD4^+$ T cells traffic through secondary lymphoid tissues in a relentless search for cognate Ags that have been transported from the periphery to the T zone by soluble transport or by dendritic cell (DC)[3] immigrants (1, 2). Under the influence of pathogen-specific "danger signals" that enhance presentation of peptide MHC (pMHC) and costimulation by DCs, recognition of pMHC by Ag-specific TCR results in T cell activation, proliferation, and effector response (3, 4). In vitro studies have shown that the earliest step in this Ag-specific T cell response involves adhesion to DCs and formation of a contact zone, followed rapidly by a TCR signaling cascade that triggers elevation of cytosolic $Ca^{2+}$ concentration ($[Ca^{2+}]_i$) (5–9). In the absence of Ag, T cells can also adhere to DCs with subsequent formation of contact zones, but the resultant $Ca^{2+}$ signals are infrequent, transient, and weak (7, 10, 11).

$Ca^{2+}$ signals have been studied in T cells using a variety of in vitro preparations, including two-dimensional culture and three-dimensional (3D) collagen gel matrix systems, in response to stimulation by mitogen, soluble ligands, pMHC delivered on lipid bilayers, or APC conjugation. These experiments revealed a heterogeneity of $Ca^{2+}$ signals ranging from transient peaks, through oscillations, to sustained plateaus (7, 9, 12–16). $Ca^{2+}$ signaling triggers lymphocyte activation by modulating gene transcription through $Ca^{2+}$-dependent regulation of nuclear transcription factors and that in turn shapes the outcome of the immune response (12, 17–19). Furthermore, variations in $[Ca^{2+}]_i$ signal modality and strength have been correlated with acute differences in T cell motility and polarization, as well as differences in stability of the immunological synapse between T cells and APC (9, 20, 21). The diversity in patterns and intensities of $Ca^{2+}$ signaling may be explained in part by differences in the type of stimulation used, the agonist strength of the peptide Ag, the subset and activation state of T cells or cell lines used, and the type and maturation status of the APC.

A significant limitation of these in vitro experiments, however, is that they fail to appropriately replicate the physiological scaffolding and environment in which T cell-DC interactions normally occur. Whereas T cell adhesion to substrates or DCs heightens the sensitivity of Ag detection and enhances downstream signaling from the TCR (22), observations of brief T cell-DC interactions and $Ca^{2+}$ signals within a 3D collagen matrix have led to the proposal that T cell activation requires serial encounters with APCs and signal integration (11). Therefore, experiments performed within intact lymphoid tissue in the context of an acute infection are needed to clarify the modality, strength, and kinetics of $Ca^{2+}$ signals required for a productive T cell response.

Multiphoton microscopy within the lymph node (LN), using both intravital and explant preparations, has delineated the choreography between naive T cells and mature DC populations (both endogenous and exogenous) that commit the T cell to activation (23). The details of these interactions differ among studies, but a common theme involves the sequential development of discrete modes of interactions that represent evolving phases of the immune response (24–28). However, whereas several reports describe brief, stochastic, and sequential initial encounters with multiple DCs pointing to successive changes in T cells as they integrate information (24, 25, 29–31), others report rapid arrest and stable interaction of T cells on DC networks near high endothelial venules (HEV) (26). Thus, variations in T cell-DC interaction may also be attributed to DC maturation status (27) or location in the LN (24). Transient and stable interactions are both associated with antigenic stimulation, but it is unclear whether they are involved in information exchange during T cell priming.

*Department of Physiology and Biophysics, †Center for Immunology, ‡Department of Neurobiology and Behavior, University of California, Irvine, CA 92697

Received for publication March 12, 2007. Accepted for publication May 22, 2007.

The costs of publication of this article were defrayed in part by the payment of page charges. This article must therefore be hereby marked *advertisement* in accordance with 18 U.S.C. Section 1734 solely to indicate this fact.

[1] This work was supported by National Institutes of Health Grants GM-41514 (to M.D.C.) and GM-48071 (to I.P.). S.H.W. was supported by the University of California, Irvine Medical Scientist Training Program and a fellowship from the American Heart Association.

[2] Address correspondence and reprint requests to Dr. Michael D. Cahalan, University of California Irvine, 275 Irvine Hall, Box 4561, Irvine, CA 92602. E-mail address: mcahalan@uci.edu

[3] Abbreviations used in this paper: DC, dendritic cell; LN, lymph node; $[Ca^{2+}]_i$, cytosolic $Ca^{2+}$; pMHC, peptide MHC; HEV, high endothelial venule; BMDC, bone marrow-derived DC; DTH, delayed-type hypersensitivity; 3D, three dimensional; cyt, cytokine; Indo-1, 1-[2-amino-5-(6-carboxy-2-indolyl)phenoxy]-2-(2-amino-5-methylphenoxy)ethane-*N*,*N*,*N*′,*N*′-tetraacetic acid.

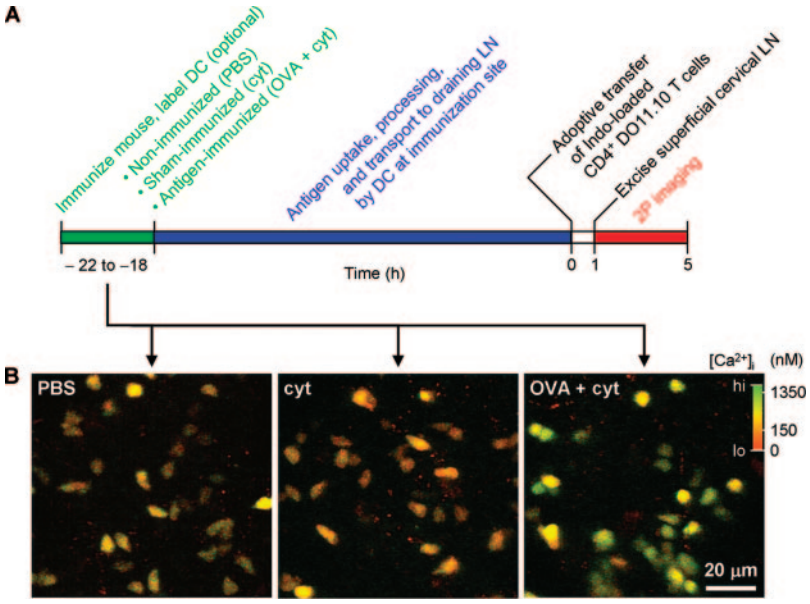


**FIGURE 1.** Experimental design. *A*, Time line of procedures for the three immunization conditions. *B*, Representative images of Ag-specific T cells in LN cortex of mice in control (nonimmunized, PBS: *left*), sham-immunized with cyt (*middle*), and Ag-immunized with OVA and cyt (OVA + cyt: *right*) conditions. $[Ca^{2+}]_i$, estimated by solution calibration of Indo-1 pentapotassium salt is represented on a pseudocolor scale from red ($Ca^{2+}$-free) to green (saturating $Ca^{2+}$). Mean $[Ca^{2+}]_i$ measurements from records associated with each snapshot were 118 ± 2 nM (PBS; $n = 402$), 107 ± 2 nM (cyt; $n = 385$), and 219 ± 2 nM (OVA + cyt; $n = 817$).

Our understanding of how these diverse interactions relate to T cell activation would be greatly enhanced by simultaneous imaging of both $Ca^{2+}$ signals and behavior of mature T cells during Ag recognition. We thus used two-photon microscopy to measure $Ca^{2+}$-dependent signals from the ratiometric fluorescent indicator 1-[2-amino-5-(6-carboxy-2-indolyl)phenoxy]-2-(2-amino-5-methylphenoxy)ethane-*N*,*N*,*N*′,*N*′-tetraacetic acid (Indo-1) during early Ag encounter of naive $CD4^+$ T lymphocytes inside LN explants. We sought to differentiate between types of $Ca^{2+}$ signaling occurring during the basal (preimmune) state, cytokine (cyt)-induced inflammatory conditions, and Ag-specific immune responses and to directly examine $Ca^{2+}$ signals elicited during T cell-DC interaction, so as to gain insight on how DCs may commit T cells to activate.

## Materials and Methods

### *Animals*

Male BALB/c and DO11.10 ($OVA_{323–339}$ peptide-specific CD4 TCR-transgenic) mice 4–10 wk of age were purchased from The Jackson Laboratory and used in accordance with protocols approved by the animal care committee (Institutional Animal Care and Use Committee).

### *Immunization and labeling of endogenous APC*

BALB/c recipient mice were immunized beneath the dorsal surface of both ears (25 μl each) and s.c. at the scruff (50 μl), with a mixture of Ag (100 or 300 μg OVA) and cyt (5 μg of FMS-like tyrosine kinase 3 ligand and 2 μg of TNF-α) in an adjuvant of 1.3% aluminum hydroxide gel adjuvant (alum, Alhydrogel; Superfos Biosector). Control mice were sham immunized with cyt and alum. In the nonimmunized controls, PBS alone was injected at the immunization sites. To label dermal DCs that traveled to draining superficial cervical LN from the injection sites, 0.5–1 μg of CFSE (Molecular Probes) was added to the immunization mixture. A similar protocol has been shown to generate a robust immune response (25), which we confirmed by showing the up-regulation of CD69 on the T cell surface within 2 and 24 h, more than seven rounds of proliferation over 3–5 days and a significant delayed-type hypersensitivity (DTH) response with Ag rechallenge (data not shown). Moreover, the addition of cyt to the immunization protocol for the imaging experiments did not alter the CD69, proliferative, or DTH profiles compared with Ag and alum alone.

### *Bone marrow-derived DCs (BMDCs)*

Bone marrow cells from the tibia and femur of BALB/c mice were cultured in supplemented medium (RPMI 1640 or IMDM), 10% FCS, and 20 ng/ml recombinant mouse GM-CSF and IL-4 (BD Pharmingen and R&D Systems, respectively). Cells were passaged as needed and used at day 8 or day 11. In some preparations, 30 ng/ml stem cell factor was added on day 0 and did not result in differences in the up-regulation of maturation markers assayed by flow cytometry. OVA was filtered and added to a portion of the culture at 1 mg/ml for ~10 h. Maturation of all cells was achieved by addition of LPS (0.5 μg/ml) to the culture medium for 16 h. Loosely adherent cells were harvested from culture, washed twice to remove Ag and cyt, stained with CellTracker Red CMTPX (Molecular Probes), and injected at multiple s.c. sites draining to both popliteal and inguinal nodes. Control cells without exposure to OVA were injected into the contralateral limb. The number of cells injected ranged between 0.2 and $2 \times 10^6$ and did not appreciably affect the density of BMDCs imaged in the T cell area of the LN at 18–24 h postinjection. For imaging purposes, we chose areas containing high densities of DCs with dendritic morphology, which were distant from the entry point in the subcapsular sinus. Bone marrow cultures (at day 11) contained >92% $CD11c^+$ cells (data not shown). Of these, >97% up-regulated maturation markers upon stimulation with LPS. Injection of BMDCs cultured with OVA plus LPS resulted in proliferation of Ag-specific KJ $1\text{-}26^+$ T cells (data not shown).

### *Adoptive transfer and sample preparation*

$CD4^+$ T cells with TCR specificity to OVA were isolated by magnetic depletion (Miltenyi Biotec) from the spleens and LN of DO11.10 TCR-transgenic mice (~9% regulatory subset). Purified T cells were incubated at 37°C in 2 μM Indo-1 pentaacetoxymethyl ester for 40 min in $CO_2$-independent medium (Invitrogen Life Technologies) and washed twice. Approximately $8–20 \times 10^6$ cells were adoptively transferred by tail vein injection into each recipient mouse 18–24 h after immunization. After allowing 40 min for homing and extravasation of T cells, superficial cervical LN were removed and kept on ice before being placed in the imaging chamber and warmed (37°C) for another 10 min ($t = 50$ min) before imaging. Little loss or compartmentalization of the $Ca^{2+}$ indicator was evident during the first 5 h after adoptive transfer.

### *Two-photon imaging*

Draining superficial cervical, popliteal, or inguinal LN explants were excised and mounted in a continuous flow chamber bathed in RPMI 1640 medium (BioWhittaker) bubbled with 95% $O_2$ and 5% $CO_2$ at 36°C. Multidimensional ($x$, $y$, $z$, time) two-photon microscopy was performed as described previously (32), with modifications for ratiometric imaging of $Ca^{2+}$-dependent fluorescence of Indo-1 (33). Femtosecond-pulsed light at 725 nm was used to excite Indo-1, and the fluorescence emission was monitored at wavelengths of 355–425 and 440–550 nm using a 440-nm dichroic mirror and 390/70 band pass and 550-nm short pass filters (Chroma Technology). The short and long wavelength Indo signals are depicted, respectively, as green and red. Increasing $[Ca^{2+}]$ results in increased short wavelength emission and decreased long wavelength emission, resulting in a shift from red to green in pseudocolored images. In some experiments, a third photomultiplier tube collected CMTPX emission (560–650 nm; but depicted blue in images). Imaging volumes (50- to 75-μm depths) with a $z$-axis resolution of 2.5 μm/step were acquired at

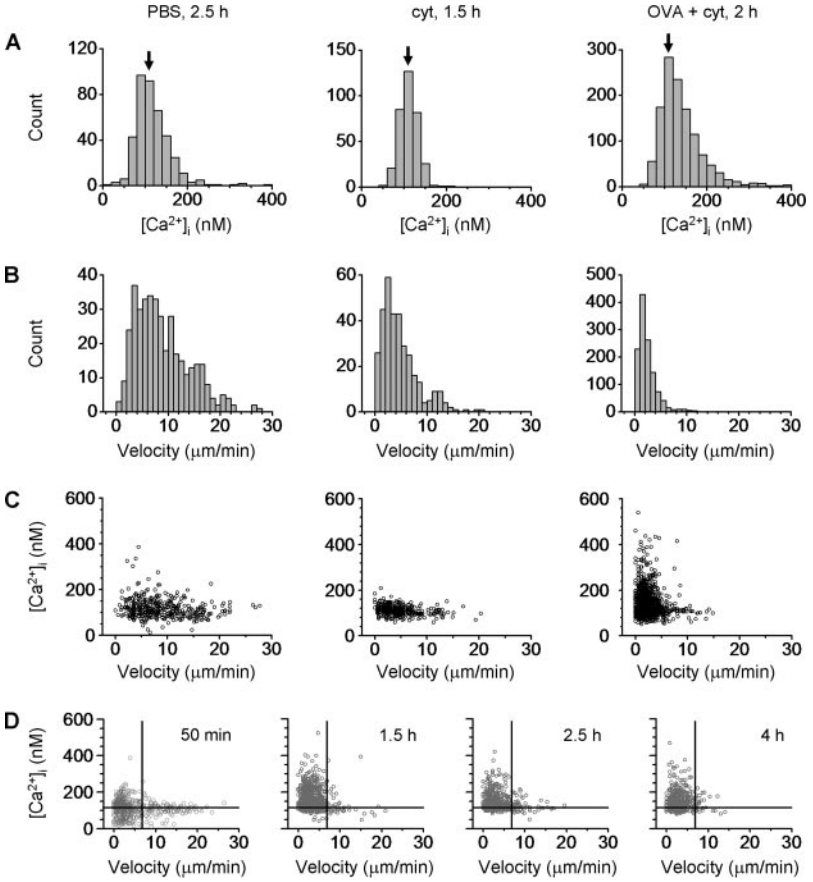


**FIGURE 2.** Population measurements of T cell motility and $[Ca^{2+}]_i$. *A*, Distributions of instantaneous $[Ca^{2+}]_i$ in nonimmunized (PBS), sham-immunized (cyt), and Ag-immunized (100 $\mu$g, OVA + cyt) conditions. Times after adoptive transfer are indicated. Arrows, duplicated in all three panels, mark the mean $[Ca^{2+}]_i$ (111 $\pm$ 1 nM, $n = 347$) under sham-immunized conditions for comparison with nonimmunized (118 $\pm$ 2 nM, $n = 402$) and Ag-immunized (143 $\pm$ 2 nM, $n = 1254$) conditions. *B*, Corresponding distributions of instantaneous T cell velocities. Mean values are: 8.8 $\pm$ 0.3 $\mu$m/min, $n = 389$ (PBS); 4.6 $\pm$ 0.2 $\mu$m/min, $n = 361$ (cyt); and 2.4 $\pm$ 0.1 $\mu$m/min, $n = 1286$ (OVA + cyt). *C*, Scatter plots, derived from the data in *A* and *B*, showing instantaneous $[Ca^{2+}]_i$ vs simultaneous measurements of T cell velocity. *D*, Changes in $[Ca^{2+}]_i$ and velocity of T cells in the superficial cervical LN of a mouse immunized with 300 $\mu$g of OVA as a function of time (indicated in hours) following adoptive transfer. Panels show scatter plots of instantaneous $[Ca^{2+}]_i$ vs velocity, as in *C*. Crosshairs, duplicated in each panel, indicate the average velocity (6.9 $\pm$ 0.2 $\mu$m/min, $n = 563$) and average $[Ca^{2+}]_i$ (112 $\pm$ 1 nM, $n = 576$) measured 2 h after adoptive transfer into a sham-immunized mouse. A distinct population of data points at the 50-min time point correlating low $[Ca^{2+}]_i$ with low velocities were measured from cells trapped within HEV that happened to be present within the imaging field.

~18- to 28-s intervals under control by MetaMorph software (Universal Imaging). Because differential scattering of short as compared with long emission wavelengths at deeper tissue depths may distort ratiometric measurements, we restricted the depths of our imaging volume, standardized the incident laser power, and limited analysis to cells of comparable signal intensity. In pilot experiments, we initially used Fura 2 for calcium measurements, but then switched to using Indo-1, which, unlike Fura 2 permits intrinsic ratiometric imaging by two-photon excitation. The qualitative patterns of calcium signals were similar with both indicators for sham- and OVA-immunized conditions (data not shown). Quantitative calibration of Indo-1 fluorescence, nevertheless, presented considerable technical difficulties due to the greater absorption and scattering of the short excitation and emission wavelengths and the requirement for accurate ratiometric measurements. We thus chose to work on excised LN, rather than intravital node preparations, because the latter exhibit diminished optical quality resulting from superficial fatty tissue and motion artifacts and for other concerns such as anesthesia and surgical trauma intrinsic to the intravital preparation (34).

### *Image processing and analysis*

Photomultiplier settings and digital image adjustments were maintained constant within each experiment to ensure consistent Indo ratio measurements. Endogenous DCs labeled with CFSE were visualized in the long wavelength Indo channel (red) but not in the short-wavelength Indo channel (green). T cell trajectories were tracked to yield centroid coordinates and velocity measurements. Average intensities of short and long wavelength Indo signals were measured at each time point for all T cells that matched acceptable criteria (intensity in both channels at least three times background and not saturated in either channel). The background-corrected ratios of short:long wavelength fluorescence (background-corrected 390:550 short-pass ratio: $R$) were then used to estimate $[Ca^{2+}]_i$ based on in vitro solution calibrations performed individually for each experiment. A $Ca^{2+}$ calibration kit (Molecular Probes) containing zero $Ca^{2+}$ (plus 10 mM EGTA) and 39.8 $\mu$M free $Ca^{2+}$ solutions was used to determine the minimal ($R_{min}$) and maximal ($R_{max}$) fluorescence of 100 $\mu$M Indo-1 pentapotassium salt (Molecular Probes), in droplets imaged by the two-photon microscope. $[Ca^{2+}]_i$ concentrations were then calibrated using the Grynkiewicz equation (35): $[Ca^{2+}]_i = K_d * S_f [(R - R_{min})/(R_{max} - R)]$, where $K_d$ was assumed to be 260 nM, and $S_f$ was the observed emission intensity ratio of the $Ca^{2+}$-free to $Ca^{2+}$-saturated Indo-1 pentaacetoxymethyl ester in the long wavelength channel.

All data are presented as mean $\pm$ 1 SEM unless otherwise noted, with statistical significance inferred by the *t* test. Throughout this manuscript, $n$ denotes the number of instantaneous $[Ca^{2+}]_i$ or velocity measurements in the experiment (representative of four experiments from each condition) corresponding to the figure, unless otherwise specified. In some analyses, $[Ca^{2+}]_i$ and velocity data from tracked cells were temporally aligned at the onset of an event such as a $[Ca^{2+}]_i$ spike, contact with or detachment from a DC. Aligned data points (with $\geq$6 events) were averaged at each time point to yield $[Ca^{2+}]_i$ and velocity traces that show temporal relationship with an event.

### *Flow cytometry*

BALB/c mice were immunized with OVA plus cyt or cyt only as described above. After 20 h, $5 \times 10^6$ $CD4^+$ DO11.10 cells were then adoptively transferred into each recipient. At various time points, cell suspensions were prepared by disruption of draining and distal LN. For both cell surface marker and proliferation assays, cells were analyzed by flow cytometry with a gate on KJ1-$26^+$ (BD Pharmingen). A CD69 FITC Ab (BD Pharmingen) was used to examine up-regulation of this early activation marker. Proliferation assays used adoptively transferred cells labeled with CFSE. To assess purity and maturity of BMDCs before injection, a portion of the bone marrow culture was set aside and stained with anti-mouse Abs to CD11c, I-A/I-E, and CD86 (eBioscience).

### *DTH characterization*

DTH responses were assayed by immunizing recipient mice in the left ear (25 $\mu$l) and scruff (75 $\mu$l) with combinations of Ag and cyt. Five $\times 10^6$ $CD4^+$ T cells from DO11.10 mice were injected 20 h after immunization. On day 7 after adoptive transfer, 20 $\mu$g of soluble OVA in 10 $\mu$l of PBS was injected into the right ear, while the contralateral ear received no injection. Twenty-four hours after Ag rechallenge, both ears were measured and the extent of swelling in the right ear compared to the left ear was used as a measure of the DTH response.

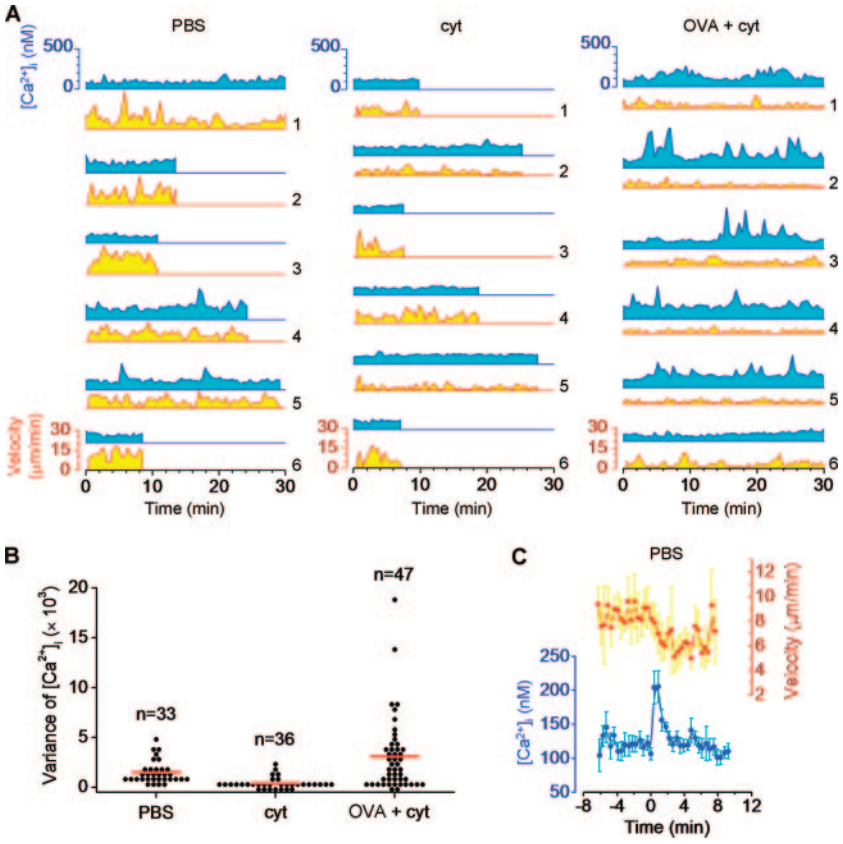


**FIGURE 3.** $Ca^{2+}$ signals and velocities of representative individual T cells. *A*, Each pair of traces shows simultaneous measurements of instantaneous $[Ca^{2+}]_i$ (blue, *top*) and instantaneous velocity (red, *bottom*) for a single T cell. Examples are shown from six cells under control (PBS), sham-immunized (cyt), and Ag-immunized (OVA + cyt) conditions. *B*, Variance of $[Ca^{2+}]_i$ (in arbitrary units) for individual cells under each immunization condition. Red horizontal bars indicate the corresponding means, which were significantly different ($p < 0.001$) among all three conditions. *C*, $[Ca^{2+}]_i$ spikes under nonimmunized conditions were associated with a slowing in T cell velocity. Traces were derived by aligning $[Ca^{2+}]_i$ spikes in 15 cells from two experiments to generate average time-aligned traces of $[Ca^{2+}]_i$ (blue, *bottom*) and corresponding velocity (red, *top*).

## Results

### *$[Ca^{2+}]_i$ is elevated in DO11.10 T cells after immunization with OVA*

We imaged naive T cells inside explanted superficial cervical LN under three conditions: 1) nonimmunized controls (PBS), 2) sham immunization with cyt, and 3) Ag immunization with OVA and cyt (OVA plus cyt). Fig. 1*A* shows our experimental protocol. CSFE was included in the adjuvant mix, so that sham or Ag immunization of BALB/c recipients resulted in fluorescently labeled DCs migrating from the injection sites to draining LN (25) (see *Materials and Methods*). One day later ($t = 0$), naive OVA-specific $CD4^+$ T cells that had been loaded with the $Ca^{2+}$ indicator Indo-1 were transferred into recipient mice. After allowing 40 min for homing to lymphoid tissue, draining LN were excised for two-photon imaging. Ratio measurements of Indo fluorescence at emission wavelengths of 355–425 and 425–550 nm were calibrated to derive $[Ca^{2+}]_i$ as described in *Materials and Methods* and are depicted on a pseudocolor scale from red (low $Ca^{2+}$) to green (high $Ca^{2+}$). Fig. 1*B* illustrates differences in $[Ca^{2+}]_i$ between T cells in the nonimmunized (PBS), sham-immunized (cyt), and Ag-immunized (OVA plus cyt) conditions at ≥2 h after adoptive transfer. The mean $[Ca^{2+}]_i$ of T cells from PBS and sham-immunized mice T cells were comparable, whereas $[Ca^{2+}]_i$ rose following Ag immunization.

### *Effects of inflammation and Ag on motility and $[Ca^{2+}]_i$ of naive $CD4^+$ T cells*

We first analyzed T cell behavior on a population basis, without regard to specific interactions with identified DCs, so as to identify possible correlations between velocity and $[Ca^{2+}]_i$ during basal motility, inflammation, and Ag recognition. $[Ca^{2+}]_i$ and velocity measurements were obtained from T cells at successive time points throughout representative imaging records beginning >50 min after adoptive transfer under the three immunization conditions (video S1).[4] A real-time graphic illustration of $[Ca^{2+}]_i$ signaling is provided to illustrate the relationship between changes in Indo-1 fluorescence and the measured $Ca^{2+}$ signal (video S2). In the absence of cognate Ag (PBS and cyt conditions), the distribution of $[Ca^{2+}]_i$ measurements centered around 110–120 nM, whereas $[Ca^{2+}]_i$ skewed markedly toward higher values after immunization with specific Ag (Fig. 2*A*). Despite having little effect on $[Ca^{2+}]_i$, inflammation resulting from sham immunization with cyt reduced the peak and average velocities of T cells compared with nonimmunized control (PBS). Ag immunization (OVA plus cyt) decreased velocities even further than with inflammation alone (Fig. 2*B*). Instantaneous T cell velocity was unrelated to $[Ca^{2+}]_i$ in control and inflammatory conditions; but in the presence of cognate Ag (OVA plus cyt) the lowest instantaneous velocities were often associated with striking increases in $[Ca^{2+}]_i$ (Fig. 2*C*). Thus, there are clear distinctions in T cell motility and $[Ca^{2+}]_i$ among control (PBS), inflammatory, and Ag-priming conditions. Inflammation reduced basal motility while having little effect on $[Ca^{2+}]_i$, whereas Ag exerted dual effects to reduce motility and increase $[Ca^{2+}]_i$. Together, inflammation and cognate Ag suppress stochastic T cell motility in an additive manner.

### *Time course of Ag-dependent changes in T cell velocity and $[Ca^{2+}]_i$*

Next, we attempted to determine whether sequential exposure to Ag was necessary before T cells could arrest and undergo robust $Ca^{2+}$ signaling. Fig. 2*D* shows scatter plots of $[Ca^{2+}]_i$ vs T cell velocity at various times after adoptive transfer into immunized

[4] The online version of this article contains supplemental material.

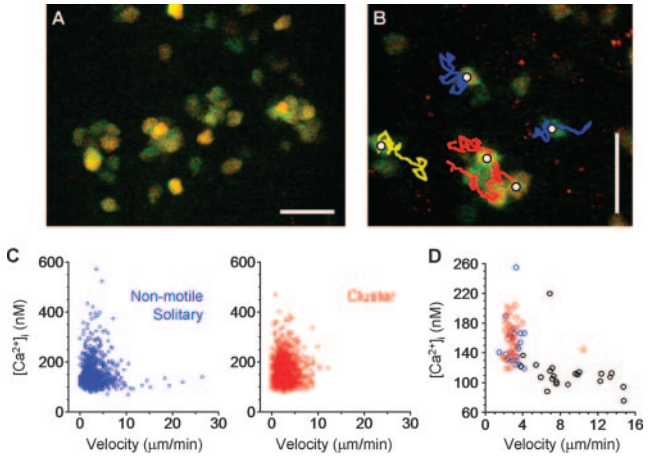


**FIGURE 4.** T cell behavior during Ag-dependent signaling inside the draining LN. *A*, Snapshot showing several clusters of T cells, as well as isolated cells in the LN of a mouse immunized with 300 $\mu$g of OVA. Note the wide variation in $[Ca^{2+}]_i$ between cells within clusters. The image is a maximal intensity projection through a 75-$\mu$m deep volume, taken from video S4, and was obtained 3 h after adoptive transfer. Scale bar, 20 $\mu$m. *B*, Snapshot of T cells in the same LN as *A*, taken 1.5 h after adoptive transfer with superimposed cell tracks (18.6-min duration) illustrating representative motilities of clustered (red tracks) and nonmotile/solitary (blue tracks) T cells. The yellow track shows the path of a cell that moved from one cluster to another. Scale bar, 20 $\mu$m. See video S5. *C*, Scatter plot of instantaneous $[Ca^{2+}]_i$ and velocity measurements of nonmotile/solitary (blue, *left*) and clustered T cells (red, *right*), obtained in a single LN. *D*, Scatter plot showing average $[Ca^{2+}]_i$ vs average velocity for individual T cells from imaging records analyzed in *C*. Each data point represents mean values for an individual T cell, classified as nonmotile/solitary (blue), and clustered (red). Motile (black) T cells, mostly from early time points, are included for comparison. Mean values for these groups were: nonmotile/solitary, 152 $\pm$ 6 nM and 3.0 $\pm$ 0.1 $\mu$m/min, 22 cells; clustered, 159 $\pm$ 4 nM and 3.0 $\pm$ 0.2 $\mu$m/min; 34 cells, and motile, 113 $\pm$ 6 nM and 8.9 $\pm$ 0.7 $\mu$m/min; 22 cells. Mean $[Ca^{2+}]_i$ and velocities were not significantly different ($p = 0.34$ and 0.78, respectively) between the nonmotile/solitary and clustered groups, but both of these groups were significantly different from motile cells ($p < 0.013$).

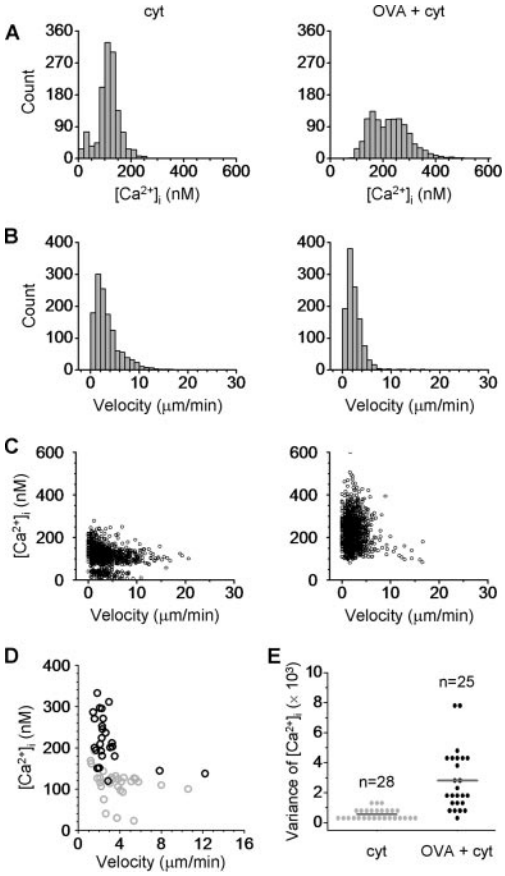


**FIGURE 5.** $[Ca^{2+}]_i$ and motility of T cells that contacted labeled DCs in sham- and Ag-immunized (OVA + cyt) conditions. *A*, Distributions of instantaneous $[Ca^{2+}]_i$. Mean values were 114 $\pm$ 2 nM (cyt; $n = 1161$) and 225 $\pm$ 2 nM (OVA + cyt; $n = 1161$). *B*, Corresponding histograms of instantaneous velocities. Mean values were 3.4 $\pm$ 0.1 $\mu$m/min (cyt; $n = 1291$) and 2.4 $\pm$ 0.1 $\mu$m/min (OVA + cyt; $n = 1144$). *C*, Scatter plots of instantaneous $[Ca^{2+}]_i$ vs velocity; subpopulation in cyt condition with low $[Ca^{2+}]_i$ and velocity are attributed to cells trapped within HEV. *D*, Scatter plot of mean $[Ca^{2+}]_i$ vs mean velocity of individual cells pooled from four experiments for sham-immunized (gray) and Ag-immunized (black) conditions. *E*, Variance of $[Ca^{2+}]_i$ traces of individual cells from *D* under sham-immunized (gray) and Ag-immunized (black) conditions. Bars, mean values.

(cyt plus OVA) recipient mice. In comparison to control experiments in nodes from sham-immunized mice (marked by crosshairs in all panels of Fig. 2*D*), little change was apparent in population measurements of velocities or $[Ca^{2+}]_i$ at 50 min after adoptive transfer. The response to Ag evolved rapidly within the next 10–40 min (video S3), demonstrated by a large increase in $[Ca^{2+}]_i$ and reduction in velocity by 1.5 h, and these changes then persisted for at least another 2.5 h. Thus, early encounters with Ag may be sufficient for maintaining $[Ca^{2+}]_i$ signals.

### *$Ca^{2+}$ signaling modality of individual T cells in LN cortex*

We next examined the kinetics of individual T cells to look for specific patterns of $Ca^{2+}$ signals under control, inflammatory, and antigenic conditions. Representative $[Ca^{2+}]_i$ traces (blue) and corresponding velocity traces (red) are shown as functions of time for six T cells under each condition (Fig. 3*A*). The most obvious difference in single-cell $Ca^{2+}$ signals was a markedly greater frequency of $[Ca^{2+}]_i$ spike transients under antigenic conditions, as demonstrated by an increase in variance of the $[Ca^{2+}]_i$ fluctuations (Fig. 3*B*). These $Ca^{2+}$ spikes were usually irregular, lacked a clear periodicity, and persisted in T cell populations for many hours after adoptive transfer. Infrequent $[Ca^{2+}]_i$ spikes were seen under nonimmunized (PBS) conditions but, surprisingly, their occurrence was even lower under inflammatory (cyt) conditions, as confirmed by a decrease in signal variance (Fig. 3*B*). $[Ca^{2+}]_i$"trough" levels, calculated as the average of minimum $[Ca^{2+}]_i$ values over 5-min intervals throughout each trace, were similar for nonimmunized and sham-immunized conditions (85.6 $\pm$ 5.6 nM, $n = 32$ cells and 92.4 $\pm$ 2.5 nM, $n = 34$ cells, respectively; $p = 0.29$), but were significantly increased to 125.2 $\pm$ 2.5 nM ($n = 56$ cells, $p < 0.001$) by immunization with 100 $\mu$g OVA.

### *$[Ca^{2+}]_i$ transients during basal motility are associated with reduced velocity*

We consistently observed T cells that displayed spontaneous $Ca^{2+}$ spikes, even in the absence of cognate Ag. To determine whether these $[Ca^{2+}]_i$ transients were accompanied by changes in T cell motility, we averaged the velocity traces from several cells after time-aligning them to synchronize the rising phase of $Ca^{2+}$ peaks. In the case of basal motility under control (PBS) conditions, this revealed a consistent reduction in velocity beginning roughly coincident with a rise in $[Ca^{2+}]_i$ that persisted even after the re-establishment of baseline $[Ca^{2+}]_i$ (Fig. 3*C*). Similar analyses under sham- and Ag-immunized conditions, however, failed to reveal

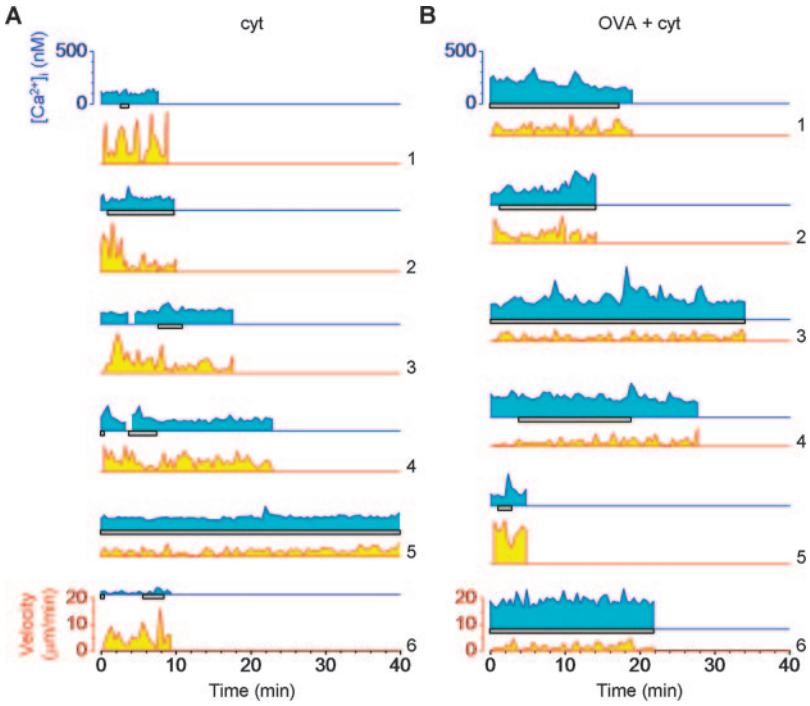


**FIGURE 6.** Instantaneous $[Ca^{2+}]_i$ signals and velocities of six representative T cells during contact with endogenously labeled DCs under sham-immunized (*A*; cyt) and antigenic (*B*; OVA + cyt) conditions. Each pair of traces shows simultaneous measurements of instantaneous $[Ca^{2+}]_i$ (blue; *top*) and velocity (red; *bottom*) for a single T cell. Durations of contacts with labeled DCs are indicated by gray bars.

any clear correlation between $[Ca^{2+}]_i$ and velocity (data not shown), possibly because motility was already low in both cases.

### *T cell behavior during Ag-dependent signaling*

Previous live-cell imaging studies have reported formation of Ag-specific T cell clusters under priming conditions (24, 25, 29, 32, 36). Soon after T cells were adoptively transferred into Ag-primed mice, we observed the development of robust, dynamic clusters within LN. Clusters were initially sparse in LN at 50 min after adoptive transfer, but their size and density increased consistently with time while the proportion of motile cells decreased. T cells within clusters exhibited $Ca^{2+}$ spiking for the entire duration of the imaging records (>30 min) (Fig. 4*A* and video S4).

Under antigenic conditions, T cells could be categorized into three groups according to their location and motility (Fig. 4*B* and video S5): 1) clustered cells (an aggregation of ≥2 cells persisting >5 min); 2) solitary, but nonmotile cells distinct from clusters (classified as showing peak instantaneous velocities <10 μm/min, and making no contacts with other T cells for >5 min); and 3) motile cells (showing instantaneous velocity >10 μm/min at least every 5 min). A comparison between nonmotile/solitary T cells and those within clusters revealed that both were similar in their instantaneous $[Ca^{2+}]_i$ and velocity distributions (Fig. 4*C*), but were distinctly different from the motile cells (● in Fig. 4*D*) that were more common at earlier time points and displayed high mean velocities and low mean $[Ca^{2+}]_i$. Although clustering of T cells has been associated with Ag recognition and activation (32), the lack of cluster formation does not predict the quality of calcium signaling.

### *$Ca^{2+}$ signaling and motility of T cells interacting with identified endogenous DCs*

The results presented above were obtained without selecting for T cells that were contacting identified DCs. We then proceeded to study $Ca^{2+}$ signaling and motility of T cells while directly visualizing interactions of T cells with endogenously labeled DCs that had been recruited from the immunization site under both sham-immunized (cyt) and Ag-immunized (cyt plus 100 or 300 μg of OVA) conditions.

Measurements of $[Ca^{2+}]_i$ in selected populations of T cells that contacted labeled DCs showed dramatic elevations under antigenic conditions as compared with those of sham immunization (Fig. 5*A*). This effect was also greater than for population measurements of T cells (Fig. 2*A*) or even T cells within clusters in experiments without visualization of DCs (Fig. 4, *C* and *D*). T cells that visibly engaged DCs also had slower velocities after sham immunization as compared with nonimmunized conditions, and their velocities decreased yet further after Ag immunization (Fig. 5*B*). Elevated $[Ca^{2+}]_i$ levels were associated with the lowest velocities for both instantaneous measurements (Fig. 5*C*) and averaged values of individual cells (Fig. 5*D*), especially after Ag immunization. The variance of individual $[Ca^{2+}]_i$ traces from T cells that contacted Ag-exposed DCs was appreciably greater than that of corresponding sham-immunized experiments (Fig. 5*E*; $p = 1 \times 10^{-5}$), indicative of an increase in frequency of $Ca^{2+}$ spiking (Fig. 6). Thus, T cells that were identified as contacting labeled migrant DCs exhibited qualitatively similar, but quantitatively more pronounced signaling and motility characteristics as compared with the overall population of nonselected cells under antigenic conditions.

### *$Ca^{2+}$ transients and visualized DC contacts*

Next, we looked at $Ca^{2+}$ signals of individual T cells during interaction with endogenously labeled DCs. Sham immunization resulted in brief contacts with visualized DCs (20 of 28 contacts had durations <4 min) that were sometimes associated with transient $Ca^{2+}$ peaks (Fig. 6*A*; *right panel* of video S6). Overall, however, these $Ca^{2+}$ traces showed low peak amplitudes and baseline trough levels (88 ± 8 nM, $n = 12$ cells, two experiments) that were little different from that observed in the absence of identified DC contact.

Immunization with OVA promoted more prolonged interactions with identified DCs (20 of 21 contacts had durations >4 min) and stable contacts with DCs often persisted throughout the entire duration of our imaging, regardless of whether the DC was migrating

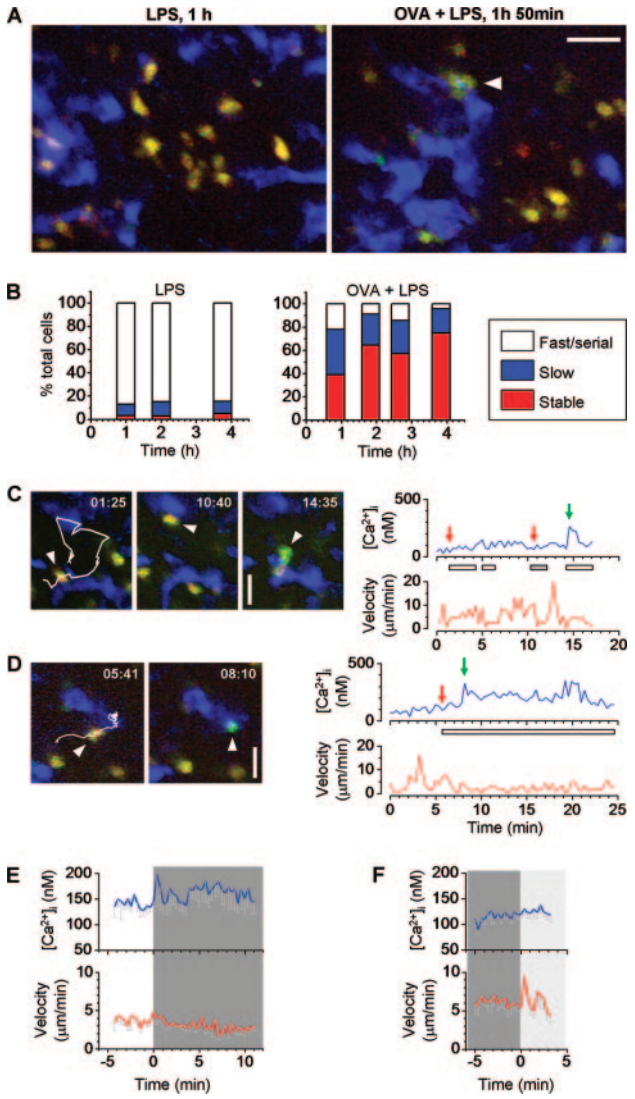


**FIGURE 7.** $Ca^{2+}$ signaling and motility of T cells during interaction with BMDCs. *A*, Maximum intensity projections showing T cells (Indo loaded, red to green) interacting with homed BMDCs (blue) that were treated with LPS alone (*left*) or OVA and LPS (*right*). Images were obtained at times following adoptive transfer of T cells as indicated. The white arrowhead at right (OVA + LPS) marks a T cell cluster. Scale bar, 20 $\mu$m. *B*, Bar graphs show the percentages of T cells displaying different modes of motility and interaction as a function of time following adoptive transfer of T cells in the presence of BMDCs treated with LPS alone (*left*) or LPS + OVA (*right*). Three classifications were made: round, nonmotile cells showing stable DC interactions (stable, red), cells with restricted motility that undergo either transient or no visible BMDC interactions (slow, blue), and cells with fast velocity undergoing serial interactions with BMDCs (fast/serial, white). *C*, Time-lapse sequence illustrating the interactions of individual Indo-loaded T cells with BMDCs (blue) treated with LPS alone (see video S9). Tracks of selected T cells are shown as overlays in the first panels. Elapsed time is indicated at the *top right* (min:s). Scale bar, 10 $\mu$m. The $[Ca^{2+}]_i$ and velocity traces of the T cell marked by the white arrowhead are displayed at the *right* as a function of time, with contacts to one or more BMDCs indicated by gray scale bars. Arrows are color-coded to represent low (red) and high (green) concentrations of $[Ca^{2+}]_i$ and correspond to the times indicated in each image snapshot. *D*, Corresponding image sequence and representative $[Ca^{2+}]_i$ and velocity traces for interactions with BMDCs pulsed with OVA and LPS (see video S10). *E* and *F*, Averages (more than six cells) of $[Ca^{2+}]_i$ (blue) and velocity (red) traces formed after time alignment with respect to the initiation of contact with BMDCs in the OVA + LPS condition (*E*) and the detachment of T cells from BMDCs in the LPS condition (*F*). Error bars, SEM. Gray shading shows duration of contact with BMDCs.

or stationary (video S7). Contacts were associated with frequent, irregular $Ca^{2+}$ spiking, usually superimposed on top of a sustained elevation in basal $[Ca^{2+}]_i$ (Fig. 6*B*). $Ca^{2+}$ spike amplitudes were greater (381 ± 29 nM, $n = 23$ cells) than in sham-immunized conditions (175 ± 11 nM, $n = 24$ cells), and the mean trough levels (169 ± 11 nM, $n = 12$ cells) were significantly greater than the sham $Ca^{2+}$ baseline (88 ± 8 nM, $n = 12$ cells) (Fig. 6*B*). Initiation and termination of DC contacts were not obviously associated with any consistent pattern of $[Ca^{2+}]_i$ signaling (Fig. 6 and video S8), even when recordings were started soon after adoptive transfer, thereby increasing the likelihood that we captured the early interaction between a T cell and DC.

### *$Ca^{2+}$ signaling during interactions with exogenous DCs*

The experiments described above using endogenously labeled DCs had limitations, in that labeled DCs were sparse (only one or a few per imaging volume) and because T cells may have interacted with Ag-presenting, but unlabeled DCs. We therefore additionally studied $Ca^{2+}$ signals in T cells during interactions with BMDCs that were pulsed with Ag, matured with LPS and fluorescently labeled before s.c. injection (see *Materials and Methods*). This approach had advantages of increasing the numbers of labeled, Ag-presenting DCs within the LN and of restricting exposure of soluble Ag to the brightly fluorescent, nearly uniform population of mature BMDCs.

Imaging was performed 18–24 h after injection of BMDCs, when both unpulsed (control, LPS) and Ag-pulsed BMDCs (OVA plus LPS) congregated in areas of the T cell zone at high density where they interacted with Indo-labeled T cells. In the absence of Ag, rapidly motile T cells engaged BMDCs serially and maintained low overall $[Ca^{2+}]_i$ (*left panels*, Fig. 7, *A* and *B*; video S9). In contrast, a large proportion of T cells showed stable interactions with Ag-pulsed BMDCs as early as 50 min following adoptive transfer, and this proportion increased further with time (*right panels*, Fig. 7, *A* and *B*; video S10). Of 173 cells, 15 (8.7%) were observed to detach from BMDCs after an initial period of contact. During this period of detachment, nine cells (60% of observed detachments) continued to undergo calcium spikes (video S11). In total, we recorded from 66 cells during periods when they were not in visualized contact with BMDC contact, and 35 (53%) of these displayed calcium spikes. Similar to the results with endogenously labeled DCs (Fig. 6), the frequency and amplitude of $Ca^{2+}$ spikes, and $Ca^{2+}$ trough levels all increased in the presence of Ag, whereas cell velocities were slowed (Fig. 7, *C* and *D*; cumulative traces not shown). Examination of individual events failed to reveal any clear association between $[Ca^{2+}]_i$ and contact with BMDCs for either unpulsed (Fig. 7*C*) or Ag-pulsed conditions (Fig. 7*D*). However, after aligning and averaging traces with respect to the initiation and detachment of contacts, a small mean elevation of T cell $[Ca^{2+}]_i$, became evident at the onset of contact with Ag-pulsed BMDCs (Fig. 7*E*). No comparable change in averaged $[Ca^{2+}]_i$, was evident on detachment from Ag-bearing BMDCs (data not shown) or unpulsed BMDCs, although in the latter case synchronized fluctuations in velocity were evident (Fig. 7*F*).

## Discussion

We used two-photon microscopy to study $Ca^{2+}$ signaling and cell motility of naive $CD4^+$ T cells engaging DCs within intact, excised LN under basal, inflammatory, and immunizing conditions. In the absence of Ag, small $Ca^{2+}$ transients occurred infrequently and were associated with prolonged decreases in velocity. The

presence of Ag further reduced T cell velocity compared with inflammation alone, which suggests that both TCR-dependent (intracellular signaling) and TCR-independent factors (i.e., maturation and density of DCs) induce T cell arrest in vivo. During early Ag encounter, marked increases in the frequency of irregular $Ca^{2+}$ spiking and small elevations of trough $[Ca^{2+}]_i$ levels were observed as early as 50 min after adoptive transfer of T cells. This experimental time point captures T cells soon after homing to the LN, suggesting that T cells have the propensity to undergo prolonged arrest and $Ca^{2+}$ signaling on or soon after initial Ag encounter. Most T cells then arrested and engaged for several hours in contacts with DCs in stable yet dynamic clusters. $[Ca^{2+}]_i$ signals continued to show irregular spikes superimposed on an elevated baseline throughout this time, but no clear changes were evident when T cells contacted or dissociated from Ag-bearing DCs. These findings in explanted LN are likely to be representative of the normal physiological situation, as previous in vivo imaging studies in nodes retaining blood and lymphatic circulation have shown that lymphocyte motility and region-specific migration patterns are closely comparable to results in explant preparations (32, 37, 38).

Because our antigenic conditions resulted in near-complete T cell proliferation in the draining LN and establishment of effector function (data not shown), it is likely that these persistent, irregular $[Ca^{2+}]_i$ fluctuations contribute importantly to T cell activation. However, we cannot exclude the possibility that initial contacts of newly homed T cells with DCs may have evoked larger $[Ca^{2+}]_i$ transients before we were able to begin imaging the node. Despite this, we have found that $Ca^{2+}$ signaling of T cells in lymphoid tissue was strikingly different from many previous in vitro observations. Increased irregularity and unpredictability in signaling is likely due to the dynamic nature of T cell interactions with APC under more physiological concentrations of Ag, in a 3D, highly cellular environment.

Several in vitro systems have been used to study $Ca^{2+}$ signaling during lymphocyte activation, revealing a wide diversity of signaling modes (39); including irregular and periodic oscillations, steady elevations, and abrupt, transient increases (5, 12–14, 19, 40). Important questions include whether the cell is able to decode all of these different modes and the nature of the activating signal under physiological conditions in the native tissue environment. NFAT, NF-κB, and AP-1 are among the most important transcription factor families involved in T cell activation, and all are regulated in a $Ca^{2+}$-dependent manner (41). It has been proposed that gene transcription is activated more efficiently by $Ca^{2+}$ oscillations than by sustained elevations of an equivalent mean level and that specificity among different transcription factors is encoded by the magnitude (18) and frequency of $Ca^{2+}$ elevations (42). For example, human $CD4^+$ T cell clones showed $Ca^{2+}$ oscillations and elevated basal $[Ca^{2+}]_i$ after encountering Ag presented by APC that were distinguished from Ag-independent $Ca^{2+}$ signals by their increased magnitude and greater spike frequency (7). Our findings are consistent with this signaling pattern in that $Ca^{2+}$ signals under antigenic conditions were distinguished from basal signals primarily by a persistent increase in variance of irregular fluctuations superimposed on modestly elevated plateau levels. In vitro studies showing high amplitude (>800 nM) calcium rises and regularly periodic oscillations may thus be atypical of responses in situ. $Ca^{2+}$ signaling by other immune cells has also been examined in previous in situ imaging studies. In thymocytes, irregular oscillations persisting >2 h, with peaks of 300–1000 nM have been reported to act as a stop signal during positive selection, although APC were not directly observed (33). A recent intravital imaging study showed an immediate increase in $[Ca^{2+}]_i$ on contact between MD4 B cells and DCs presenting Ag followed by prolonged arrest (43).

Comparison to in vitro $[Ca^{2+}]_i$ measurements in naive $CD4^+$ T cells suggests that the $[Ca^{2+}]_i$ signals in situ correspond to stimulation by ~10–100 pMHC complexes, a level too low to induce $Ca^{2+}$ flux by types of APC other than DCs, and on the steep part of the dose-response relation between $Ca^{2+}$ signaling and number of pMHC (6). Thus, the range of $[Ca^{2+}]_i$ signaling in the LN likely represents an optimal compromise between high sensitivity for detection of rare Ags and saturation of $Ca^{2+}$ signaling that may result in tolerance or anergy through activation of NFAT unopposed by AP-1 (44, 45). The oscillatory $Ca^{2+}$ signals observed in vitro must persist for >1 h in order for the T cell to commit to a program of activation (17). Concordant with this, the irregular $Ca^{2+}$ signals we observed in situ persisted throughout the duration of our imaging records (~45 min) and probably much longer, suggesting that T cells may integrate $Ca^{2+}$ signals over prolonged periods to distinguish antigenic conditions from the infrequent $Ca^{2+}$ spikes seen in the absence of Ag.

Another difference between in vitro and in situ observations concerns the association between $Ca^{2+}$ signals and contacts with APC. Stimulation of TCR in vitro through Ag presentation results in almost immediate activation of $Ca^{2+}$ signaling, which then subsides rapidly following removal of the stimulus (9, 40). In 3D collagen gel matrices, $[Ca^{2+}]_i$ in DO11.10 T cells rose 30–180 s after contact with OVA-pulsed DCs, was maintained while T cells crawled over the DC surface, and fell back to baseline on detachment (11). In contrast, although our in situ observations revealed an average elevation of T cell $[Ca^{2+}]_i$ during contact with identified Ag-presenting DCs, individual records generally showed no obvious changes in $[Ca^{2+}]_i$ associated with contact or dissociation from DCs. In particular, $Ca^{2+}$ signaling persisted in the absence of identified contact with labeled DCs (e.g., videos S8 and S11). One possibility is that T cells may be exposed to Ag in the LN even in the absence of visualized contact with labeled DCs; e.g., by contact with fine DC dendrites below the limit of our resolution, by transfer of pMHC from DC to T cell (21), by communication within the dense network of resident DCs (46, 47), or by Ag spread among DCs by mechanisms such as uptake of cellular debris or exosomes (1, 48, 49). Alternatively, $Ca^{2+}$ signaling in T cells within the LN may require only sporadic contacts with Ag-bearing DCs to initiate an intrinsic signaling pathway that remains active for an appreciable time even in the absence of Ag (50). Regardless of the specific mechanism, it is clear that Ag conditions lead to irregular $Ca^{2+}$ spikes at higher amplitude and frequency that are clearly distinct from the intermittent basal $Ca^{2+}$ spikes occurring in the absence of Ag. Thus, persistent and irregular $Ca^{2+}$ signaling likely represent the physiological stimulus for T cell activation.

## Acknowledgments

We thank Dr. Mark Miller for his participation in early stages of this investigation and Mark Ilagan for help with cell culture and flow cytometry.

## Disclosures

The authors have no financial conflict of interest.

## References

1. Itano, A. A., and M. K. Jenkins. 2003. Antigen presentation to naive CD4 T cells in the lymph node. *Nat. Immunol.* 4: 733–739.
2. Trombetta, E. S., and I. Mellman. 2005. Cell biology of antigen processing in vitro and in vivo. *Annu. Rev. Immunol.* 23: 975–1028.
3. Guermonprez, P., J. Valladeau, L. Zitvogel, C. Thery, and S. Amigorena. 2002. Antigen presentation and T cell stimulation by dendritic cells. *Annu. Rev. Immunol.* 20: 621–667.
4. Sallusto, F., and A. Lanzavecchia. 2002. The instructive role of dendritic cells on T-cell responses. *Arthritis Res.* 4(Suppl. 3): S127–S132.

5. Delon, J., N. Bercovici, R. Liblau, and A. Trautmann. 1998. Imaging antigen recognition by naive $CD4^+$ T cells: compulsory cytoskeletal alterations for the triggering of an intracellular calcium response. *Eur. J. Immunol.* 28: 716–729.
6. Delon, J., N. Bercovici, G. Raposo, R. Liblau, and A. Trautmann. 1998. Antigen-dependent and -independent $Ca^{2+}$ responses triggered in T cells by dendritic cells compared with B cells. *J. Exp. Med.* 188: 1473–1484.
7. Montes, M., D. McIlroy, A. Hosmalin, and A. Trautmann. 1999. Calcium responses elicited in human T cells and dendritic cells by cell-cell interaction and soluble ligands. *Int. Immunol.* 11: 561–568.
8. Donnadieu, E., G. Bismuth, and A. Trautmann. 1994. Antigen recognition by helper T cells elicits a sequence of distinct changes of their shape and intracellular calcium. *Curr. Biol.* 4: 584–595.
9. Negulescu, P. A., T. B. Krasieva, A. Khan, H. H. Kerschbaum, and M. D. Cahalan. 1996. Polarity of T cell shape, motility, and sensitivity to antigen. *Immunity* 4: 421–430.
10. Revy, P., M. Sospedra, B. Barbour, and A. Trautmann. 2001. Functional antigen-independent synapses formed between T cells and dendritic cells. *Nat. Immunol.* 2: 925–931.
11. Gunzer, M., A. Schafer, S. Borgmann, S. Grabbe, K. S. Zanker, E. B. Brocker, E. Kampgen, and P. Friedl. 2000. Antigen presentation in extracellular matrix: interactions of T cells with dendritic cells are dynamic, short lived, and sequential. *Immunity* 13: 323–332.
12. Lewis, R. S., and M. D. Cahalan. 1989. Mitogen-induced oscillations of cytosolic $Ca^{2+}$ and transmembrane $Ca^{2+}$ current in human leukemic T cells. *Cell Regul.* 1: 99–112.
13. Hess, S. D., M. Oortgiesen, and M. D. Cahalan. 1993. Calcium oscillations in human T and natural killer cells depend upon membrane potential and calcium influx. *J. Immunol.* 150: 2620–2633.
14. Wulfing, C., J. D. Rabinowitz, C. Beeson, M. D. Sjaastad, H. M. McConnell, and M. M. Davis. 1997. Kinetics and extent of T cell activation as measured with the calcium signal. *J. Exp. Med.* 185: 1815–1825.
15. Feske, S., J. Giltnane, R. Dolmetsch, L. M. Staudt, and A. Rao. 2001. Gene regulation mediated by calcium signals in T lymphocytes. *Nat. Immunol.* 2: 316–324.
16. Irvine, D. J., M. A. Purbhoo, M. Krogsgaard, and M. M. Davis. 2002. Direct observation of ligand recognition by T cells. *Nature* 419: 845–849.
17. Negulescu, P. A., N. Shastri, and M. D. Cahalan. 1994. Intracellular calcium dependence of gene expression in single T lymphocytes. *Proc. Natl. Acad. Sci. USA* 91: 2873–2877.
18. Dolmetsch, R. E., R. S. Lewis, C. C. Goodnow, and J. I. Healy. 1997. Differential activation of transcription factors induced by $Ca^{2+}$ response amplitude and duration. *Nature* 386: 855–858.
19. Lewis, R. S. 2003. Calcium oscillations in T-cells: mechanisms and consequences for gene expression. *Biochem. Soc. Trans.* 31: 925–929.
20. Friedl, P., and E. B. Brocker. 2002. TCR triggering on the move: diversity of T-cell interactions with antigen-presenting cells. *Immunol. Rev.* 186: 83–89.
21. Wetzel, S. A., T. W. McKeithan, and D. C. Parker. 2002. Live-cell dynamics and the role of costimulation in immunological synapse formation. *J. Immunol.* 169: 6092–6101.
22. Randriamampita, C., G. Boulla, P. Revy, F. Lemaitre, and A. Trautmann. 2003. T cell adhesion lowers the threshold for antigen detection. *Eur. J. Immunol.* 33: 1215–1223.
23. Cahalan, M. D., and I. Parker. 2006. Imaging the choreography of lymphocyte trafficking and the immune response. *Curr. Opin. Immunol.* 18: 476–482.
24. Mempel, T. R., S. E. Henrickson, and U. H. Von Andrian. 2004. T-cell priming by dendritic cells in lymph nodes occurs in three distinct phases. *Nature* 427: 154–159.
25. Miller, M. J., O. Safrina, I. Parker, and M. D. Cahalan. 2004. Imaging the single cell dynamics of $CD4^+$ T cell activation by dendritic cells in lymph nodes. *J. Exp. Med.* 200: 847–856.
26. Shakhar, G., R. L. Lindquist, D. Skokos, D. Dudziak, J. H. Huang, M. C. Nussenzweig, and M. L. Dustin. 2005. Stable T cell-dendritic cell interactions precede the development of both tolerance and immunity in vivo. *Nat. Immunol.* 6: 707–714.
27. Hugues, S., L. Fetler, L. Bonifaz, J. Helft, F. Amblard, and S. Amigorena. 2004. Distinct T cell dynamics in lymph nodes during the induction of tolerance and immunity. *Nat. Immunol.* 5: 1235–1242.
28. Stoll, S., J. Delon, T. M. Brotz, and R. N. Germain. 2002. Dynamic imaging of T cell-dendritic cell interactions in lymph nodes. *Science* 296: 1873–1876.
29. Bousso, P., and E. Robey. 2003. Dynamics of $CD8^+$ T cell priming by dendritic cells in intact lymph nodes. *Nat. Immunol.* 4: 579–585.
30. Gunzer, M., C. Weishaupt, A. Hillmer, Y. Basoglu, P. Friedl, K. E. Dittmar, W. Kolanus, G. Varga, and S. Grabbe. 2004. A spectrum of biophysical interaction modes between T cells and different antigen-presenting cells during priming in 3-D collagen and in vivo. *Blood* 104: 2801–2809.
31. Celli, S., Z. Garcia, and P. Bousso. 2005. CD4 T cells integrate signals delivered during successive DC encounters in vivo. *J. Exp. Med.* 202: 1271–1278.
32. Miller, M. J., S. H. Wei, I. Parker, and M. D. Cahalan. 2002. Two-photon imaging of lymphocyte motility and antigen response in intact lymph node. *Science* 296: 1869–1873.
33. Bhakta, N. R., D. Y. Oh, and R. S. Lewis. 2005. Calcium oscillations regulate thymocyte motility during positive selection in the three-dimensional thymic environment. *Nat. Immunol.* 6: 143–151.
34. Germain, R. N., M. J. Miller, M. L. Dustin, and M. C. Nussenzweig. 2006. Dynamic imaging of the immune system: progress, pitfalls and promise. *Nat. Rev. Immunol.* 6: 497–507.
35. Grynkiewicz, G., M. Poenie, and R. Y. Tsien. 1985. A new generation of $Ca^{2+}$ indicators with greatly improved fluorescence properties. *J. Biol. Chem.* 260: 3440–3450.
36. Ingulli, E., A. Mondino, A. Khoruts, and M. K. Jenkins. 1997. In vivo detection of dendritic cell antigen presentation to $CD4^+$ T cells. *J. Exp. Med.* 185: 2133–2141.
37. Miller, M. J., S. H. Wei, M. D. Cahalan, and I. Parker. 2003. Autonomous T cell trafficking examined in vivo with intravital two-photon microscopy. *Proc. Natl. Acad. Sci. USA* 100: 2604–2609.
38. Huang, A. Y., H. Qi, and R. N. Germain. 2004. Illuminating the landscape of in vivo immunity: insights from dynamic in situ imaging of secondary lymphoid tissues. *Immunity* 21: 331–339.
39. Quintana, A., D. Griesemer, E. C. Schwarz, and M. Hoth. 2005. Calcium-dependent activation of T-lymphocytes. *Pflügers Arch.* 450: 1–12.
40. Donnadieu, E., D. Cefai, Y. P. Tan, G. Paresys, G. Bismuth, and A. Trautmann. 1992. Imaging early steps of human T cell activation by antigen-presenting cells. *J. Immunol.* 148: 2643–2653.
41. Isakov, N., and A. Altman. 2002. Protein kinase C$\theta$ in T cell activation. *Annu. Rev. Immunol.* 20: 761–794.
42. Dolmetsch, R. E., K. Xu, and R. S. Lewis. 1998. Calcium oscillations increase the efficiency and specificity of gene expression. *Nature* 392: 933–936.
43. Qi, H., J. G. Egen, A. Y. Huang, and R. N. Germain. 2006. Extrafollicular activation of lymph node B cells by antigen-bearing dendritic cells. *Science* 312: 1672–1676.
44. Macian, F., F. Garcia-Cozar, S. H. Im, H. F. Horton, M. C. Byrne, and A. Rao. 2002. Transcriptional mechanisms underlying lymphocyte tolerance. *Cell* 109: 719–731.
45. Heissmeyer, V., F. Macian, R. Varma, S. H. Im, F. Garcia-Cozar, H. F. Horton, M. C. Byrne, S. Feske, K. Venuprasad, H. Gu, et al. 2005. A molecular dissection of lymphocyte unresponsiveness induced by sustained calcium signalling. *Novartis Found. Symp.* 267: 165–174.
46. Lindquist, R. L., G. Shakhar, D. Dudziak, H. Wardemann, T. Eisenreich, M. L. Dustin, and M. C. Nussenzweig. 2004. Visualizing dendritic cell networks in vivo. *Nat. Immunol.* 5: 1243–1250.
47. Watkins, S. C., and R. D. Salter. 2005. Functional connectivity between immune cells mediated by tunneling nanotubules. *Immunity* 23: 309–318.
48. Carbone, F. R., G. T. Belz, and W. R. Heath. 2004. Transfer of antigen between migrating and lymph node-resident DCs in peripheral T-cell tolerance and immunity. *Trends Immunol.* 25: 655–658.
49. Thery, C., L. Duban, E. Segura, P. Veron, O. Lantz, and S. Amigorena. 2002. Indirect activation of naive $CD4^+$ T cells by dendritic cell-derived exosomes. *Nat. Immunol.* 3: 1156–1162.
50. Costello, P. S., M. Gallagher, and D. A. Cantrell. 2002. Sustained and dynamic inositol lipid metabolism inside and outside the immunological synapse. *Nat. Immunol.* 3: 1082–1089.